

Robust image restoration for ground-based space surveillance

Douglas A. Hope, Michael Hart, Stuart M. Jefferies and James Nagy

Hart Scientific Consulting International LLC, 6135 N. Tucson Mountain Dr., Tucson, AZ 85743

ABSTRACT

Myopic deconvolution from wave front sensing (MDWFS) is a powerful tool for high-resolution imaging. It is typically used with monochromatic, short exposure images with integration times less than the coherence time for the atmosphere, and Shack-Hartmann wave-front sensor data where the number of sub-apertures across the pupil is commensurate with the turbulence strength D/r_0 where D is the diameter of the telescope and r_0 is the spatial coherence length of the atmosphere. However, there are important imaging scenarios that do not fit this model. Imaging faint targets usually requires integration times greater than the atmospheric coherence time and large spectral bandwidths. Observing targets during poor seeing conditions results in D/r_0 values that are significantly greater than the number of sub-apertures across the pupil. In these cases, we may expect that a high fidelity estimate of the object will require an algorithm that accurately models the physical effects of broad temporal and spectral bandwidth in the point-spread function.

In this paper we demonstrate the performance of a new MDWFS algorithm, called DORA, designed to work with imagery obtained in strong turbulence conditions. This algorithm includes models of the temporal behavior of the atmosphere and finite spectral bandwidth. It includes several stages of processing, including DWFS and joint estimation via multi-frame blind deconvolution (MFBD). Results based on simulated data show that DORA will provide high-fidelity restorations for imagery acquired through strong turbulence conditions, $D/r_0 > 40$. Real-world performance of the new code is established with results from data acquired with the AEOS 3.6 m telescope both with and without adaptive optics compensation.

1 INTRODUCTION

To obtain the full performance of an imaging system when viewing through the Earth's atmosphere requires careful mitigation of the turbulence-induced aberration in the observed wave fronts. This is typically achieved through a combination of adaptive optics (AO) and post-detection numerical processing. In the numerical processing step, the quality of a restored image depends on the accuracy with which we know the point-spread function (PSF) for the observation. When little (or no) information is available on the PSF it becomes necessary to turn to non-linear, multi-frame blind deconvolution (MFBD) techniques to find estimates for both the blur-free object and the PSF [1].

MFBD is ill-posed, because the underlying mathematical model is ill-conditioned, and so is susceptible to entrapment in local minima in the parameter hyperspace during the optimization process. When that happens, the result is a poor restoration. Unfortunately, the number of local minima increases rapidly with increasing atmospheric turbulence and entrapment becomes almost certain at turbulence strengths of $D/r_0 > 40$ (here D is the diameter of the telescope aperture and r_0 is the spatial coherence length of the atmosphere). This is a serious limitation as it severely restricts sky access for Space Situational Awareness. For example, at Mt Haleakala in Hawaii, the median nighttime seeing has $r_0 \sim 15$ cm at zenith and even in I band where r_0 is somewhat larger, MFBD is only effective for observations down to a zenith angle of ~ 60 degrees.

For MFBD to be useful in stronger turbulence regimes it is important to reduce the number of local minima in the problem. An effective way to do so is to use high-cadence wave-front sensor (WFS) data, acquired simultaneously with the focal plane image, during the restoration process. The WFS data then provide a strong constraint on the wave front (and thus PSF) during the modeling. We note that joint modeling of the focal plane and WFS data is known as myopic deconvolution [2]. In this way, we are able to take advantage of existing hardware on telescopes such as AEOS that are equipped with an AO system.

2 ALGORITHM BACKGROUND

As we discuss in Jefferies et al. [3], high spatial frequency aberrations of the wave-front phase become increasingly damaging to image quality as the seeing worsens. These terms rapidly come to dominate the PSF, and so their

accurate estimation becomes critical to successful image restoration. A loss of fidelity at high spatial frequencies in the wave front results in PSF models with a morphology that differs greatly from the true atmospheric PSFs.

There are two important changes in the morphology of the PSFs. First, with the absence of high spatial frequencies in the wave front the faint speckles in the wings of the PSF all but vanish. If these speckles are not well modeled by the restoration code, restored target estimates will suffer from background fog that may mask nearby debris or microsatellites. In cases where the true background signal is high, the absence of these faint speckles will be less important, because they will be swamped by shot noise. However, changes in the morphology of the bright PSF speckles will prove disastrous for the restoration. The problem of missing high spatial frequencies is not usually of concern when restoring imagery from moderate turbulence, i.e. $D/r_0 < 20$, which is typically the operating regime of current algorithms in the literature. However, as the turbulence strength increases the changes in the PSF morphology increase as shown Figure 1 where the root-mean-square error (RMSE) of an ensemble of PSFs before and after filtering out the high spatial frequencies of the wave-front is plotted vs. turbulence strength.

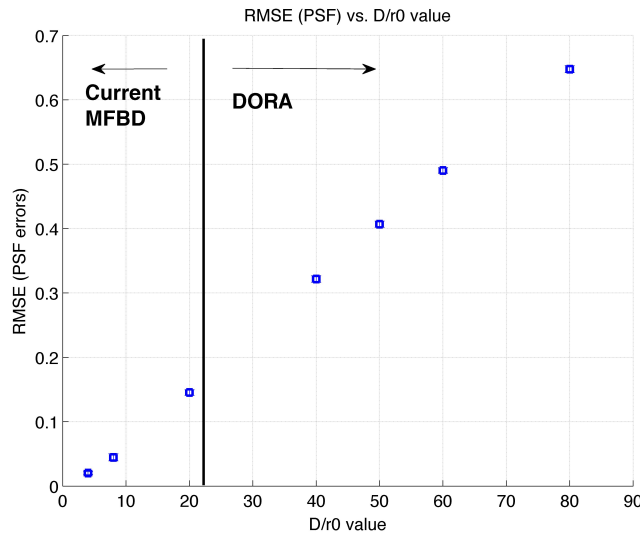


Figure 1. Plotted as a function of D/r_0 is the RMS difference between instantaneous monochromatic PSFs computed from wave-front phases before and after filtering out the highest spatial frequencies.

We have developed DORA, a new algorithm [4] that is designed to address regimes of poor seeing that go beyond the capabilities of existing MFBD algorithms. The algorithm does so by including WFS measurements as constraints on the wave-front phase estimates as well as short-exposure focal plane images. It also incorporates a complete Fourier optical model of the forward imaging problem to model the temporal and spectral integrations that occur in broad-band focal plane images.

DORA estimates the critical high spatial frequencies of the wave front by taking into account the fact that the turbulence above most ground-based imaging systems can be characterized by well-separated layers of frozen turbulence with different velocity vectors (the frozen flow model, FFM) [5]. Studies of the atmosphere at Mt. Haleakala have suggested that there are typically 2-3 such layers [6].

The FFM requires that we know the wind velocities of all significant layers of turbulence in the atmosphere. These are computed from an autocorrelation of the WFS measurements, which are captured at a cadence that substantially exceeds the Greenwood frequency and therefore capture the effects of frame-to-frame coherence in the wave front. The calculated wave-front slopes are stacked into a data cube as shown in Figure 2, and the 3D spatio-temporal autocorrelation of the cube is calculated. Consider the effect of a wave front characterized by a single frozen layer moving across the pupil. The strongest signal will occur at the center of the autocorrelation cube, at zero spatial and temporal lags. But as time progresses, and the wave front advances across the aperture, the strongest correlation signal will be seen at a spatial lag equal to the elapsed time multiplied by the wind vector. The signature of a frozen layer is thus a line of strong signal projecting from the origin of the autocorrelation cube whose direction corresponds to the direction and speed of the corresponding wind, illustrated in Figure 3. The strength of the correlation signal is directly related to the strength of turbulence in the layer, and the rate of decay with temporal lag indicates the degree to which the layer is not in fact well represented as a frozen flow.

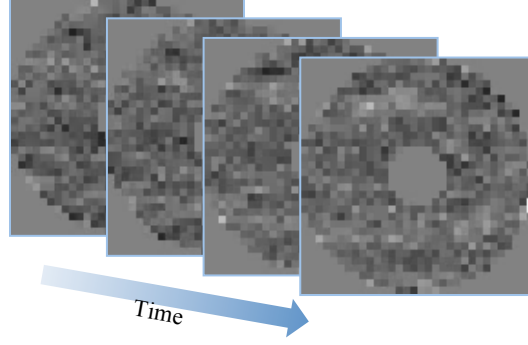


Figure 2. Measured WFS slope data from the AEOS telescope arranged in spatio-temporal sequence.

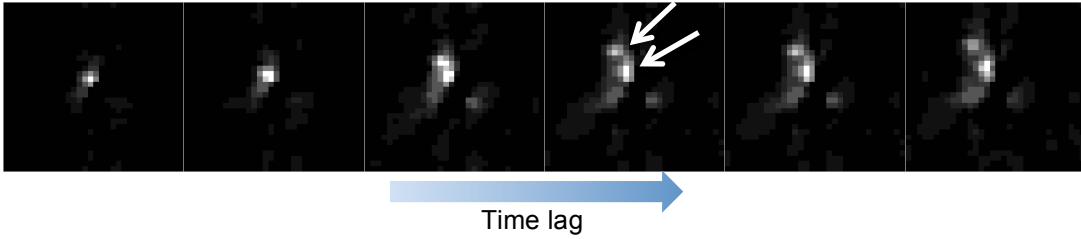


Figure 3. Consecutive time-lag slices from the 3D autocorrelation of the data in Figure 2. Two frozen layers, noted by the arrows in frame 4, are detected as spots of high signal projecting from the origin.

The pupil wave front $\Phi(x, t + \Delta t)$ is modeled as a sum of independent static turbulent layers:

$$\Phi(x, t + \Delta t) = \sum_i \alpha_i(x - v_i \Delta t, t),$$

where v_i denotes the velocity of the i^{th} layer. Using the FFM results in better sampling of the high-spatial frequencies of the wave front. This is illustratively shown in Figure 4 where in each successive time slot the wave front phase has moved some physical distance in the pupil.

The measured WFS data, as illustrated in the top row of Figure 4, is related to the unknown, better-sampled composite grid, illustrated in the bottom panel of Figure 4, by a sequence of linear operations. We first use the wind vectors to define operators that model the motion of each of the atmospheric layers. With the frozen flow assumption, one can consider the atmospheric layers to behave like rigid objects, and thus the motion can be accurately described, using the wind vectors, by linear affine transformations. The second and third linear operations involve, respectively, extracting pupil aperture regions from the fine, composite grid, and down sampling of each individual frame from the fine to the coarse grid. Putting these operations together, the FFM phase reconstruction problem requires solving a large-scale (regularized) linear least squares problem; details of the mathematical model are given in [7], and a parallel implementation is described in [8].

Note that the fine grid information obtained through the FFM phase reconstructor provides much better sampling of the wave front phases. This additional information is essential to pick up high frequency information that is not picked up by the individual frames of coarse grid WFS data.

The use of WFS data in the restoration process dictates the use of the Fourier optics model for the atmospheric PSF. The instantaneous speckle PSF $h(\mathbf{x}; \lambda, t)$ is the inverse Fourier transform of the optical transfer function (OTF) which is the autoconvolution

$$\hat{H}(\mathbf{u}; \lambda, t) = B_w(\mathbf{u}; \lambda) \hat{\Phi}_k(\mathbf{u}; \lambda, t) \odot B_w(-\mathbf{u}; \lambda) \hat{\Phi}_k^*(-\mathbf{u}; \lambda, t)$$

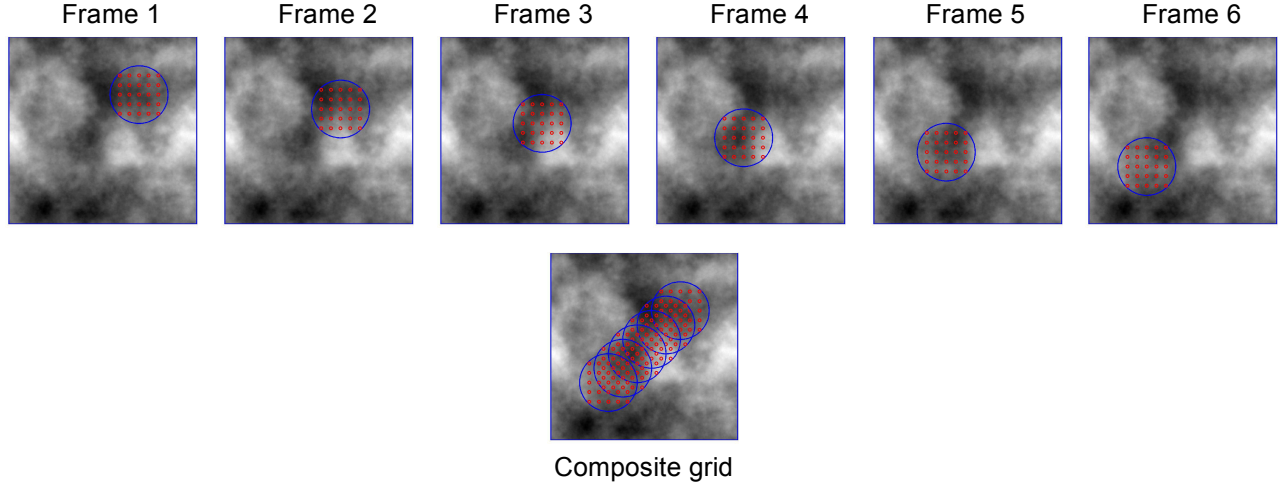


Figure 4. Estimates of the wave-front phase are built from consecutive snapshots (top row) on a composite grid that spans an elongated phase screen (bottom panel) sampled by the aperture as the frozen layer is advected over the pupil by the wind.

where $B(\mathbf{u};\lambda)$ is a binary pupil support mask at wavelength channel λ and $\Phi(\mathbf{u};\lambda,t)$ is the optical path difference modeled by the FFM, scaled and resampled to the pupil size associated with the wavelength λ at time k , \odot denotes convolution and $*$ denotes complex conjugation. This model ensures that $h(\mathbf{x};\lambda,t)$ is a non-negative, band-limited function. Also, we have assumed that atmospheric scintillation is negligible. The spectrally and temporally integrated PSF is computed as

$$h(\mathbf{x}) = \iint h(\mathbf{x};\lambda,t) d\lambda dt$$

The integrals over time and wavelength represent the spectral and temporal bandwidth associated with the observation. This description for the PSF is widely used for the restoration of images acquired through atmospheric turbulence. However, it is typically used with the assumption of negligible spectral and temporal bandwidth that is only applicable for monochromatic speckle images for which the integration time of the observation is comparable to the atmospheric coherence time. When the model is applied to scenarios where there is wavelength and/or temporal integration the model is only approximately valid. How good the approximation is depends on the turbulence strength.

This is illustrated in Figure 5 which shows a conceptual 3D parameter space of spectral bandwidth, integration time, and turbulence strength. Within this space, simulated PSFs are shown for two turbulence regimes, low turbulence of $D/r_0=10$ and strong turbulence of $D/r_0 = 40$. Each has been computed also with two levels of spectral bandwidth (zero and 50%) and temporal integration (zero and 32 ms) for a total of 8 cases. Typically the space of MFBF problems that can be solved using a Fourier optics model falls below $D/r_0=10$: in this regime, the quad panel in Figure 5 for the low turbulence case shows that finite spectral and temporal bandwidths have only modest effects on the PSF. By contrast, in the panel for the high turbulence case, both spectral and temporal integrations individually as well as both together show strong effects. Using the WFS measurements and the FFM for the wave front extends the space of accessible MFBF problems to $D/r_0 = 50$ [5].

3 ALGORITHM

Our algorithm assumes that the field of view is small. In this case we can focus on isoplanatic, incoherent imagery and model the focal plane data, $g_k(x)$, as a convolution between the object intensity distribution $f(x)$, and an atmospheric point-spread function $h_k(x)$ that does not depend on the field position x .

An important foundation of DORA is the correct physical modeling of constraints on the atmospheric PSF. The algorithm minimizes a metric that measures both the fit between the focal plane data and the data model (referred to

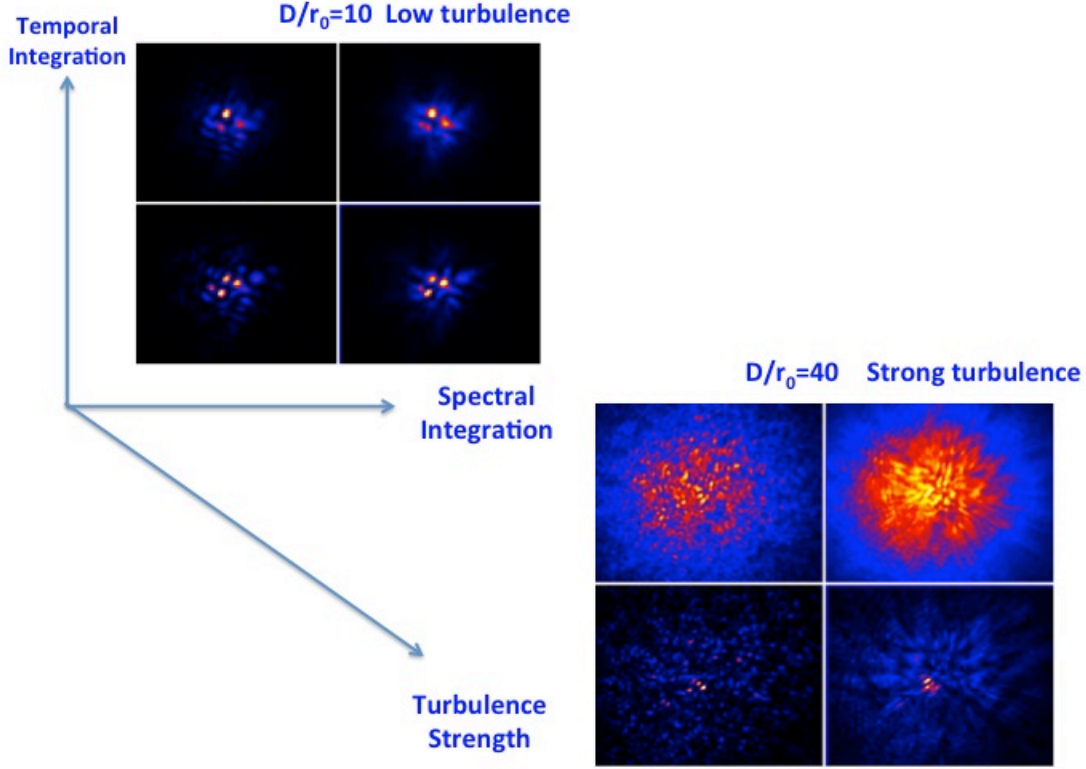


Figure 5. Shown are temporally and spectrally integrated PSFs for two regimes of atmospheric turbulence. In the low turbulence regime at $D/r_0=10$ a modest effect of temporal integration is evident by the change in the morphology of the speckles. In the strong turbulence regime both temporal and spectral integrations dramatically change the morphology of the PSFs. In each panel from lower left clockwise: instantaneous-monochromatic; temporally integrated-monochromatic; temporal and polychromatic; and instantaneous polychromatic. The temporal integration time is 32 ms; the polychromatic bandwidth is 50%.

as the convolution metric) and a fit between the measured and modeled wave-front gradients (WFS metric). The

$$\text{convolution metric is defined as } \varepsilon = \sum_k \sum_{\mathbf{x}} d_k(\mathbf{x}) |g_k(\mathbf{x}) - \hat{g}_k(\mathbf{x})|^2$$

where the subscript k denotes the timeslot and \mathbf{x} denotes the pixel location in the focal plane. The WFS metric is defined as

$$\varepsilon_{WFS} = \sum_k \sum_j \sum_{\mathbf{x}} M \left[\left(\nabla^x \Phi_{jk}(\mathbf{x}) - S_{jk}^x \right)^2 + \left(\nabla^y \Phi_{jk}(\mathbf{x}) - S_{jk}^y \right)^2 \right]$$

where the index j denotes the set of WFS time slots that correspond to data frame k . The data model is computed as the convolution of the PSF estimate for the k -th data frame and the object estimate,

$$\hat{g}_k(x) = \sum_{x'} \hat{f}(x - x') \hat{h}_k(x')$$

The PSF is computed directly from the estimated wave-front phases at each turbulent layer. At the central wavelength and for each time slot j the phases are punched out of the elongated phase screens estimated from the FFM and an instantaneous PSF is computed. Temporal integration is accomplished by adding the PSFs $h_{k,jw}(\mathbf{x})$ computed at each time index j . For each data frame k , the time index spans the number of WFS frames that fall within a single integration time of the imaging camera. To compute the spectral integration, the phases at the central wavelength are up-sampled to a pupil size determined by the ratio of wavelength w to the central wavelength. The phase values are also scaled by the same ratio. The spectrally and temporally integrated PSF

$$h(\mathbf{x}) = \int \int h(\mathbf{x}; \lambda, t) d\lambda dt$$

is approximated by computing the instantaneous speckle PSF at a series of discrete wavelengths (color planes) and time slots. These are then summed across all color planes and time slots,

$$\hat{h}_{k,j}(\mathbf{x}) = \sum_w \hat{h}_{k,jw}(\mathbf{x}).$$

DORA offers a choice of two methods for estimating the object. First, the object can be estimated using a Wiener filter (WF) parameterization of the object in terms of the wave-front phases,

$$F(u) = \frac{\sum_k \hat{H}_k^*(u) G_k(u)}{\sum_k |\hat{H}_k(u)|^2 + \gamma}$$

where $\hat{H}_k(u)$ denotes the Fourier Transform (FT) of the PSF, i.e. the optical transfer function (OTF), and $G_k(u)$ denotes the FT of the k -th image frame. The parameter γ denotes a regularization parameter that can be adjusted to mitigate the effects of noise amplification. The WF estimate is useful when the image camera completely captures the whole image, i.e. there is no image truncation. Its advantage is that it eliminates the need to explicitly estimate the object, thus reducing the number of variables to be estimated; however, it does not enforce any non-negativity constraint on the object. The alternate approach is to explicitly estimate the object while imposing a non-negativity constraint. This is accomplished by parameterizing as $\hat{f}(x) = \psi^2(x)$.

4 RESULTS

At this point we do not yet have telescope data on hand that approach seeing values as bad as $D/r_0=40$ for which DORA was designed. We have therefore tested our algorithm's performance in the strong turbulence regime with simulated observations of SEASAT under conditions of full daylight sky illumination, modeling a solar phase angle of 40° . Two cases were run, where we have assumed a challenging problem in which the satellite is changing pose rapidly, allowing just 8 frames of data to be restored before the object can no longer be considered constant. The satellite was taken to be faint, with photon noise equivalent to integrated magnitudes of 6 and 8. No detector read noise was included, but would in any case be well below the shot noise from the background. Results from the restorations are shown in Figure 6. In the case of the 6th magnitude object, the overall morphology of the satellite is well estimated, although fine details are lost to the noise. The fainter object is barely visible in a single frame of the raw data, and yet some evidence of the satellite's structure is still discernible in the restoration. These results are very encouraging for imaging faint LEO objects during the day.

Real-world performance of DORA has been addressed with data acquired with the AEOS 3.6 m telescope. Although the data presently available are limited to turbulence strengths no worse than $D/r_0 \sim 12$, they do have broad spectral bandwidth of about 25% and integration times up to an order of magnitude and more longer than the atmospheric coherence time. In Figure 7, we show a result from data recorded with the telescope's AO system running in closed loop. Even though the AO compensation is very good, with resolution approaching the diffraction limit, DORA is able to enhance the image quality further. This is because even with AO correction the WFS data still contain information on the residual wave-front errors that the AO system has not corrected; there is still strong frame-to-frame correlation in the data that can be exploited.

Figure 8 shows a different case in which the AO system was not running. This target is the Hubble Space Telescope and data were collected with integration time of 20 ms. In this example the constraints on the high spatial frequencies of the wave front and the proper modeling of the temporal integration of the PSF resulted in a restoration with sharpness comparable to the case when AO was in closed loop. The background is also cleaned up, improving the contrast in the neighborhood of the satellite.

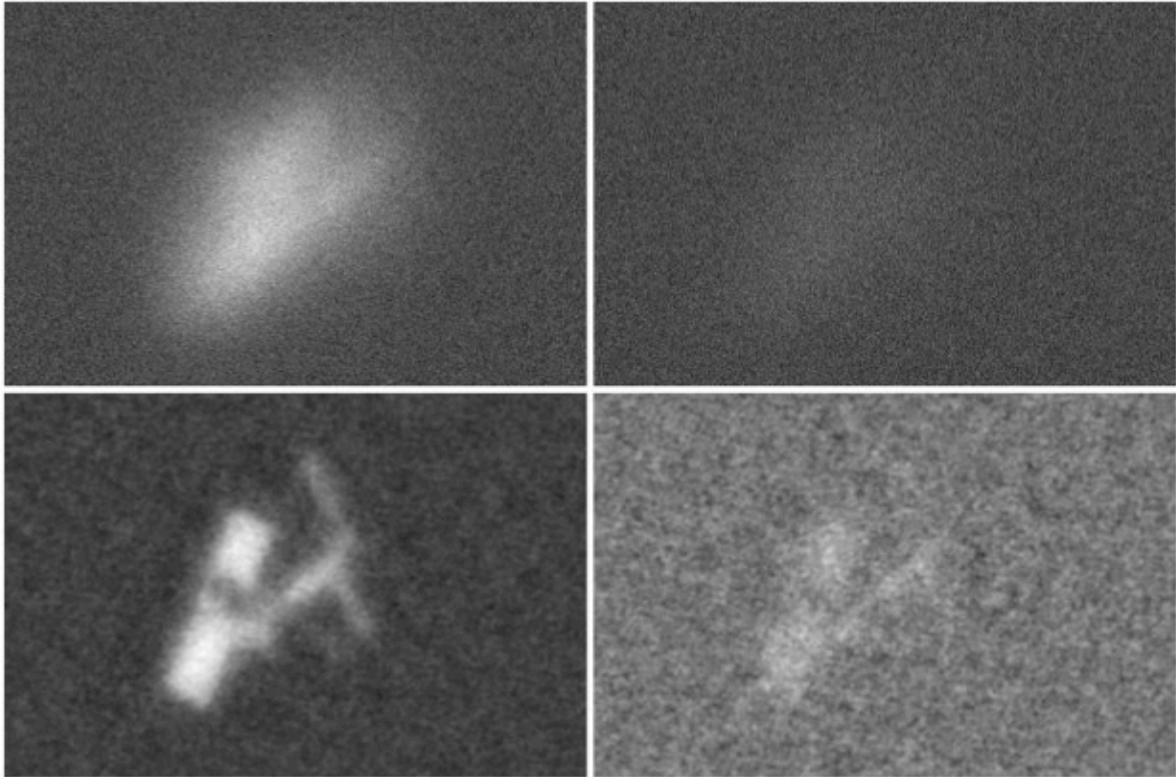


Figure 6. Restorations of simulated observations of SEASAT in daytime. (Left column) Photon noise included to simulate a target of magnitude 6. (Right column) Target scaled to magnitude 8. (Top row) Simulated data. (Bottom row) Results of DORA restoration.

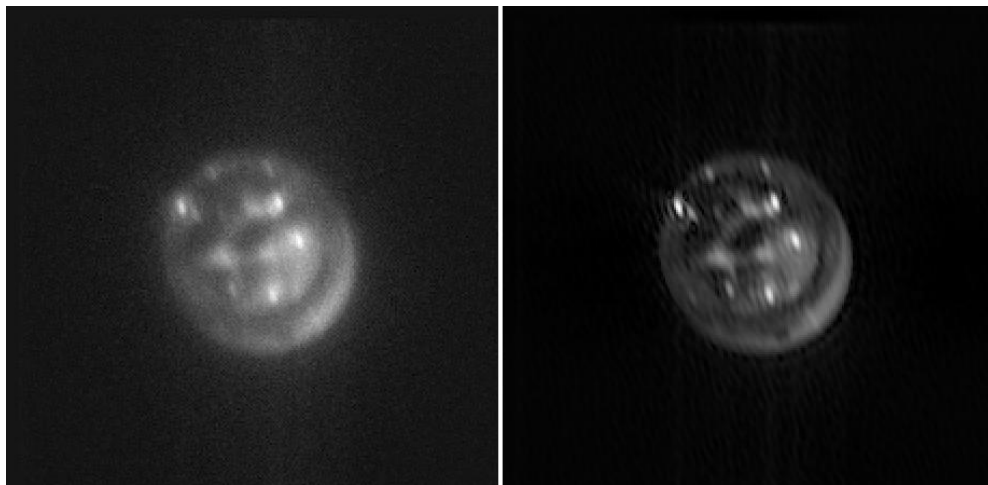


Figure 7. Ariane 5 rocket body. Left: Raw data frame with AO in closed loop (integration time of 2 ms, spectral bandwidth of 25% at $0.85 \mu\text{m}$). Right: DORA restoration using 40 frames of AO data. Both images are shown on a square root scale.

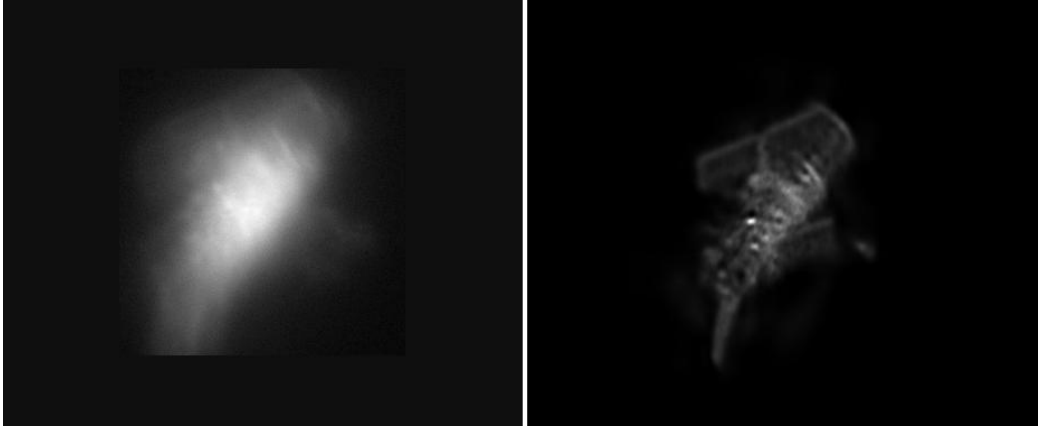


Figure 8. The Hubble Space Telescope. Left: Raw data frame with AO in open loop (integration time of 20 ms, spectral bandwidth of 25% at 0.85 μm). Right: DORA restoration using 20 frames of data.

5 CONCLUSIONS

Image restoration in the turbulence regime $D/r_0 > 20$ using existing MFBD algorithms is very challenging because of the virtual certainty of entrapment in local minima. DORA presents a new approach to MFBD in the strong turbulence regime by proper modeling of the high spatial frequencies in the wave front, enabled by constraints provided by the WFS and the use of a frozen flow model of the atmosphere. Accurate modeling of the high frequencies enables us in turn to make accurate physical models of both temporally and spectrally integrated PSFs, a capability that is important when restoring imagery obtained for large values of D/r_0 where chromatic radial streaking of the PSF speckles is a large part of the PSF morphology. By including temporal and spectral modeling, MFBD restorations spanning a larger volume of the observing space can now be solved using the Fourier optics model. This is crucial to support operational scenarios that require data collection under non-ideal conditions of strong turbulence.

6 ACKNOWLEDGEMENTS

This work has been supported by the Air Force Research Laboratory, Directed Energy Directorate, under contract FA9451-12-C-0004.

7 REFERENCES

- [1] Jefferies, S. M., and Christou, J. C., "Restoration of astronomical images by iterative blind deconvolution", *Astrophysical Journal*, **415**, 862-864 (1993)
- [2] J. Conan, L. Mugnier, T. Fusco, V. Michau, and G. Rousset, "Myopic deconvolution of adaptive optics images by use of object and point-spread function power spectra," *Appl. Opt.* 37, 4614-4622 (1998).
- [3] Jefferies, S. M., Hope, D. A., Hart, M., and Nagy, J. G., "High-resolution imaging through strong atmospheric turbulence and over wide fields-of-view," AMOS Technical Conference, Kihei, HI, (2013).
- [4] Hart, M. et al., "Multi-Frame blind deconvolution for imaging in daylight and strong turbulence conditions," *Proc. SPIE* 8165, 81650L, (2011).
- [5] Jefferies, S. M. and Hart, M., "Deconvolution from wave front sensing using the frozen flow hypothesis", *Optics Express*, 19, 1975-1984 (2011).
- [6] Rimmele, T., "Haleakala turbulence and wind profiles used for adaptive optics performance modeling", ATST Project Document RPT-0030 (2006). Chu, Q., Jefferies, S. M. and Nagy, J. G., "Iterative wave front reconstruction for astronomical imaging", *SIAM J. Sci. Computing*, in press (2013).
- [7] Kelley, K. W. and Nagy, J. G., "Parallel implementation of a frozen flow based wave-front reconstructor", AMOS Technical Conference, Kihei, HI, (2013).